

Article

Modelling the Effect of Deformation on Discontinuous Precipitation in Magnesium—Aluminium Alloy

Joseph Robson , Jiaxuan Guo  and Alec Davis 

Department of Materials, University of Manchester, Manchester M13 9PL, UK;
jiaxuan.guo@postgrad.manchester.ac.uk (J.G.); alec.davis@manchester.ac.uk (A.D.)

* Correspondence: joseph.robson@manchester.ac.uk

Abstract: Magnesium–Aluminium alloys can decompose from a supersaturated solid solution by either continuous or discontinuous precipitation. Deformation prior to precipitation has been shown to strongly suppress the discontinuous precipitation mode and promote continuous precipitation. In this work, a model is used to explore the interaction between deformation and precipitation in the Mg–Al system. It has been shown that accelerated nucleation of continuous precipitates on dislocations is predicted to have the dominant effect in suppressing discontinuous precipitation by reducing the solute supersaturation. A secondary effect is the direct role played by twins in the deformed structure, which act as impenetrable barriers to discontinuous precipitate growth. However, even in the deformed case, small regions of discontinuous precipitation are still observed. It is proposed that this is due to the high level of strain concentration expected in the grain boundary regions, which provides a locally enhanced driving force for the migration of grain boundaries such that limited discontinuous precipitation occurs before continuous precipitation becomes established.

Keywords: precipitation; theory and modelling (kinetics, transport, diffusion); magnesium alloys



Citation: Robson, J.; Guo, J.; Davis, A. Modelling the Effect of Deformation on Discontinuous Precipitation in Magnesium—Aluminium Alloy. *Alloys* **2022**, *1*, 54–69. <https://doi.org/10.3390/alloys1010005>

Academic Editor: Frank Czerwinski

Received: 11 March 2022

Accepted: 7 April 2022

Published: 11 April 2022

Publisher's Note: MDPI stays neutral with regard to jurisdictional claims in published maps and institutional affiliations.



Copyright: © 2022 by the authors. Licensee MDPI, Basel, Switzerland. This article is an open access article distributed under the terms and conditions of the Creative Commons Attribution (CC BY) license (<https://creativecommons.org/licenses/by/4.0/>).

1. Introduction

The formation of deformation resistant precipitates from a supersaturated solid solution is one of the most powerful methods of strengthening applied in alloys. The most common mode of precipitation involves the nucleation and growth of individual isolated precipitates that can provide formidable barriers to dislocation motion when shear resistant and closely spaced. When these precipitates form, there is a continuous evolution in their particle size distribution throughout the microstructure, and thus this mode is referred to as continuous precipitation (CP) [1]. However, another mode of precipitation is also possible. It is observed in over 80 binary systems under particular conditions of supersaturation and temperature [1,2]. This mode involves the cellular growth of the precipitating phase, usually as alternating layers with the matrix, behind a migrating high angle boundary (HAGB). At any moment during precipitation, the microstructure can be clearly divided into two regions; one containing precipitate phase and one which is precipitate free. This is known as discontinuous precipitation (DP). Given its morphological similarity to eutectoid transformations, it is often understood on the basis of the same essential mechanisms [3–5].

The magnesium–aluminium system is one example of a commercially important alloy type where both CP and DP are observed. Magnesium–aluminium is the basis of the dominant class of AZ magnesium alloys, such as AZ91, where precipitation can occur of a second phase referred to as β , which has an ideal stoichiometric composition $Mg_{17}Al_{12}$. Despite the ability of these alloys to form a volume fraction of precipitate close to 15%, the strengthening response obtained is poor; less than half that achieved in some aluminium alloys that form a much lower fraction of precipitates [6]. There is thus considerable interest in improving the strengthening response of AZ type alloys during precipitation. One issue that contributes to the poor strengthening response of AZ alloys to ageing is the formation

of DP. The DP lamellae are usually widely spaced and offer poor barriers to dislocation motion. In addition, since DP and CP are in competition, when DP forms, it suppresses CP, mainly by consuming the supersaturated matrix and reducing the volume available to CP [7]. Therefore, it is considered desirable to suppress DP and promote CP, and achieving this may lead to better strengthening behaviour in a temperature range that is amenable to commercial heat treatment (for example <24 h ageing time).

One method that can suppress DP and promote CP, as well as providing direct strengthening, is to perform deformation prior to precipitation. It has been demonstrated experimentally for Mg–Al under one set of conditions that deformation appears to slow down the formation of DP [8]. In this work, cold rolling to a heavy reduction of 30% was found to almost completely eliminate DP for an ageing condition that would otherwise produce a fully DP microstructure [8].

However, in general, it is known that pre-deformation can have either an accelerating or retarding effect on DP [8]. This is because DP is in competition with CP, and deformation can influence the balance of this competition. Recent studies have demonstrated that severe plastic deformation (SPD) [9,10] or cold compression [11] can accelerate and refine the formation of continuous precipitates in Mg–Al. However, even when very high cumulative strains are achieved during SPD, local regions of DP are still observed. Indeed, since DP occurs behind a migrating HAGB, the factors that promote boundary motion, such as a stored energy gradient, are also expected to promote DP and lead to a coupling between recrystallisation and discontinuous precipitation [9].

The purpose of the present work is to extend a model previously developed for competitive CP and DP in Mg–Al alloys to include the effect of pre-deformation. This model is then used to explore the possible interactions between these two precipitation modes to determine the mechanisms by which deformation can influence the fraction of each. A subset of new experiments from a wider study are used to test the model and demonstrate some of the complex interactions between deformation, twinning, and DP/CP that can occur.

2. Method

A small number of experimental results from a wider study are chosen here to illustrate important aspects of the interaction of DP and CP with deformation. The material used is commercial AZ80 alloy (nominal composition range 7.8–9.2 Al–0.2–0.8 Zn–0.12–0.5 Mn wt%, balance Mg), provided as direct chill–cast ingot by Luxfer MEL Technologies, Manchester, UK. The as cast material was homogenised at 400 °C for 24 h using an argon gas furnace, and then hot rolled on a laboratory mill at 400 °C to a total reduction of 80%. This material was then solution treated for 1 h at 420 °C, leading to a refined equiaxed grain structure with a basal texture and dissolution of the Al and Zn. Finally, cold rolling (at room temperature) was applied in 5 equi-strain passes to 5% total reduction. Greater cold rolling reductions were also investigated, but it was found that even a 5% reduction produced the desired effect in suppressing DP whilst facilitating subsequent analysis using scanning electron microscopy (SEM) and electron backscattered diffraction (EBSD). Precipitation heat treatment was carried out on both cold rolled and solution treated material for 16 h at 220 °C. This temperature was chosen since it corresponds to a condition where DP is usually dominant, enabling the effect of deformation on DP precipitation to be most clearly seen [8].

Specimens for optical and scanning electron microscopy (OM and SEM) were prepared with standard metallographic methods using acetic glycol etchant. Specimens for EBSD were not etched but subject to further polishing using a Leica EM RES102 Ion Beam Milling System operated at a current of 2.8 mA and a voltage of 7 kV, using two cleaning steps: firstly with a beam angle of 12.5° for 10 min and secondly at an angle of 5° for 10 min.

Analysis of DP fraction was performed by manually identifying DP regions and determining area fractions using ImageJ. SEM was performed using Tescan Mira 3 FEGSEM, operated at 10 kV with a working distance of 20 mm. Backscattered imaging mode was

used to provide atomic number contrast. EBSD was performed using an FEI Magellan FEG-SEM equipped with an OI NordlysS EBSD detector and AZtec software, using an accelerating voltage of 20 kV. The step size used for the EBSD scans was 0.75 μm . Maps were processed in AZtec Crystal and are presented in inverse pole figure colouring (plotting the normal direction).

3. Modelling

CP and DP are in competition, and thus promotion of one precipitation mode will tend to suppress the other. To understand this competition, a classical model was previously developed that allows the two mechanisms to occur simultaneously and naturally predicts their interactions based on the competition for solute, free volume, and boundary pinning effects. This model has been adapted in the present work to also include the effect of deformation on both CP and DP. Full details of the model as applied to non-deformed material are given elsewhere [7], but its essential features are summarized below.

- CP is modelling using a classical size-class model based on the Kampmann and Wagner numerical (KWN) framework. Classical nucleation and growth controlled by aluminium is assumed. The particles are modelled as plates with a fixed aspect ratio.
- DP is modelled assuming nucleation occurs from a certain proportion of precipitates heterogeneously nucleated on grain boundaries [12]. Growth of the DP regions is predicted using a model developed by Klinger et al. [5] that provides a unique solution to the growth velocity, based on the assumption that concentration gradients control the growth of the interlamellar α -matrix and gradients in interface curvature control growth of the β lamellar.
- CP influences DP by two effects; the reduction in supersaturation due to CP (which is modelled using a mean-field approximation) and the pinning effect of CP on the migrating DP front. Of these effects, it has been shown that the reduction in supersaturation is by far the most important [7].
- DP influences CP by reducing the free volume available in which CP can occur. This is modelled using the classical method of relating extended and real transformed volumes (Johnson–Mehl–Avrami–Kolmogorov [1]).

In the present work, this model was modified in two ways to include the effect of deformation. Firstly, the dislocations introduced by deformation are known to provide potent nucleation sites for the formation of continuously nucleated β phase. This effect is accounted for by modifying the energy barrier for nucleation $G_{het}^* = \alpha G_{hom}^*$ and the nucleation site density N_v . An approximate estimate for appropriate values for these parameters comes from the work of Ma et al. [9]. They measured both dislocation density and β particle number in a heavily deformed AZ80 alloy and compared this with an identically heat treated non-deformed case. For a measured dislocation density in the deformed state of $1.4 \pm 0.2 \times 10^{14} \text{ m}^{-2}$, they recorded a 10 fold increase in the particle number density during the early stages of ageing. Assuming coarsening was negligible, this implies a 10 fold increase in nucleation rate due to deformation. This was used to estimate the modification factor α for heterogeneous nucleation, giving a value $\alpha = 0.216$. Note that in this case, α should be considered as a fitting parameter that gives approximately the correct accelerating effect for heterogeneous nucleation on dislocations, rather than being ascribed any physical significance.

Precipitate growth will also be influenced by formation on dislocations. However, the observation that deformation leads to a much higher number density of smaller β precipitates suggests this effect is less strong than that on nucleation. This is probably because once sufficient nucleation and initial growth has occurred, it is diffusion through the matrix to the precipitate and dislocation line that becomes rate limiting, rather than diffusion along the dislocation. Furthermore, the β precipitates retain their habit plane even when precipitating on dislocations, and do not grow preferentially along the dislocation line, which limits the effect that dislocation pipe diffusion can have on their growth. For these reasons, the effect of dislocations on the precipitate growth rate was ignored. As

demonstrated later, the predicted change in precipitate size associated with introducing additional nucleation sites is consistent with that observed experimentally, suggesting this is a reasonable assumption.

Deformation will also influence DP. The DP growth front is a high angle grain boundary, migrating into supersaturated matrix. The migration of the boundary is driven by the chemical free energy change on transformation of supersaturated α to $\alpha + \beta$, but in deformed material it will be additionally driven by the stored energy in the deformation structures. DP is therefore a coupled process of precipitation and recrystallization. As discussed by Ma et al. [9], the driving force due to the supersaturation is typically much greater than that due to the dislocation substructures, and this can lead to recrystallization and DP occurring under conditions for which recrystallization alone would not occur. A full physical model for the combined DP and recrystallization process is highly complex and beyond the scope of the present work. This is because such a model would need to consider the simultaneous effects of the evolving supersaturation (due to CP) and evolving stored energy in the deformation structure due to recovery processes. Instead, in the present work, a simple approach is used that captures the effect that the additional driving force due to the deformation structure will have on the DP boundary migration velocity. The boundary velocity is the product of the mobility and driving pressure. Assuming the mobility is unchanged with deformation (which is reasonable since it is controlled by diffusion and curvature at the DP growth front), the boundary velocity may be written as:

$$v = \left(1 + \frac{P_d}{P_c}\right)v_c \quad (1)$$

where P_d is the pressure on the boundary arising from the energy in the deformation structure, P_c is the pressure on the boundary arising from the supersaturation, and v_c is the DP front growth velocity due to supersaturation alone (i.e., in the absence of deformation effects). The pressure on the boundary due to the energy stored in the dislocations is given by:

$$P_d = Gb^2\rho_d \quad (2)$$

where G is the shear modulus, b the dislocation Burgers vector ($b = 0.32$ nm [6]) and ρ_d the dislocation density. During the early stages of DP, the DP growth front will be highly curved, and this leads to a retarding pressure due to the surface tension effect. As will be shown later, this pressure is only significant when the DP region is very small, but it does become important when considering what happens in the early stages of DP growth. For the mean field model discussed here, this effect is ignored (since it is implicitly captured by the fitting of the DP nucleation rate).

Crystal Plasticity Modelling

In addition to the mean field effect of deformation, captured in the model described above, it is important to recognise that in magnesium, strain is often highly non-uniformly distributed within the microstructure. For example, digital image correlation (DIC) techniques commonly reveal that local strain concentrations, which usually occur in regions close to grain boundaries, can exceed 30 times the macroscopically applied strain [13]. As will be demonstrated later, this heterogeneity of deformation can play an important role in determining the local behaviour of a region with regard to precipitation. It is difficult to explore this experimentally for a rolled sample, but a good estimate of the non-uniform strain distribution can be obtained from a full field crystal plasticity model [14].

In the present work, the DAMASK crystal plasticity framework was used to perform simulations of the strain distribution obtained after the cold rolling step. Details of this model, and its application to magnesium alloys, are given elsewhere [14]. Simulations were run for a 3-dimensional ensemble containing 125 grains within a $128 \times 128 \times 128$ grid. The grains were produced by Voronoi tessellation from random seeds, and the orientation of each grain was assigned by random sampling of the experimentally determined texture

prior to cold rolling. This gives a reasonable representation of the true microstructure prior to the cold rolling step, and importantly captures the effect of the experimentally measured texture on strain localization.

The load was applied assuming plane strain compression, which is reasonable for rolled material away from the sheared surface layers. A strain rate of 1 s^{-1} was assumed, which is a reasonable estimate for laboratory cold rolling. The single crystal constitutive response was modelled using a phenomenological power law that accounts for all of the slip and twinning systems that are known to be active in magnesium. Further details of this law and the parameters used as inputs to the constitutive response are given in [14].

No attempt was made to refine the fitting parameters in the single crystal power law since the purpose of the present work was not to accurately predict the stress-strain response of the material, but rather to understand the extent of strain heterogeneity that would be expected after rolling. Similarly, since the geometry of twinning (i.e., the formation of multiple lenticular regions of sheared material of different orientation within a parent grain) is not captured in the crystal plasticity model [14], it is not an exact faithful reproduction of the deformed microstructure. Nevertheless, previous work has demonstrated that the strain localisation predicted by such full-field crystal plasticity models is a reasonably faithful reproduction of that measured in magnesium [14].

4. Results

4.1. Microstructural Observations

An overview of the microstructures at different stages of processing and heat treatment is shown in Figure 1. After hot rolling and solution treatment (Figure 1a) a fully recrystallized and equiaxed grain structure is obtained, as intended. Cold rolling to 5% reduction (Figure 1b) introduces a large number of twins into this microstructure. Comparing the aged microstructures with and without cold deformation (Figure 1c,d), respectively) it can be seen that as expected, the solution treated and aged microstructure appears completely invaded by DP, whereas there is much less DP in the cold rolled and aged state (although it is not completely suppressed). The twins persist after aging of the cold-rolled material. Image analysis revealed that the DP fraction was reduced from 100% in the solution treated and aged state to $23 \pm 5\%$ in the cold rolled and aged material.

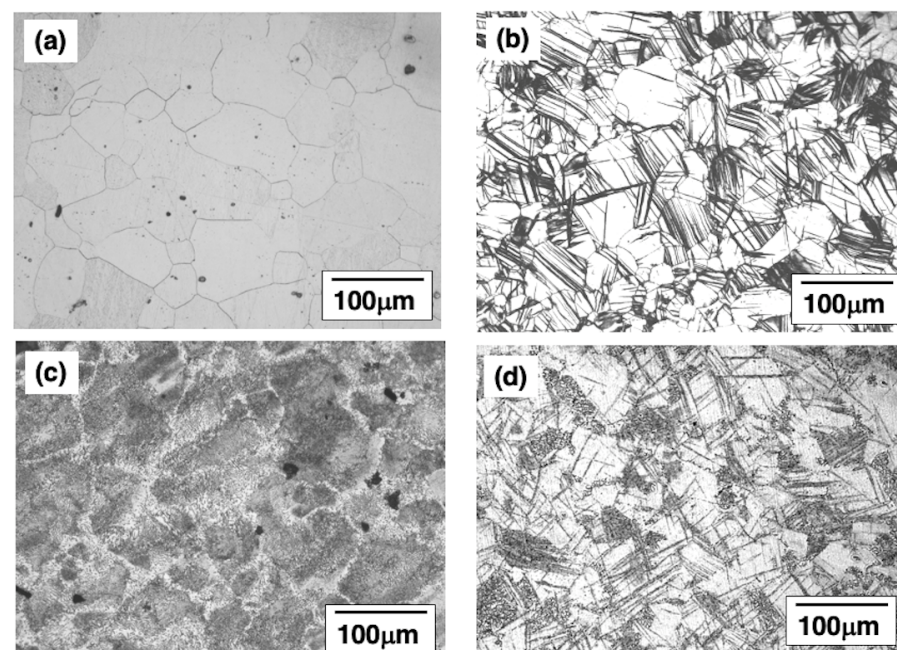


Figure 1. Optical micrographs showing (a) hot rolled and solution treated condition (b) cold rolled condition (c) condition in (a) after aging $220\text{ }^{\circ}\text{C}$, 16 h, (d) condition in (b) after aging $220\text{ }^{\circ}\text{C}$, 16 h.

Further details of the microstructure and texture of the material are revealed in the EBSD maps (Figure 2). EBSD reveals a typical strong basal texture in the hot rolled and solution treated state, but with some grains in non-basal orientations. Cold rolling produces many fine twins as evident in the optical images, but the overall texture is similar to the solution treated condition, with the basal texture being 7.4 times multiple times random (MRD) in the solution treated condition and 8.4 times MRD as cold-rolled. Quantitative analysis of the EBSD images revealed that 92% of the grains contain at least one twin in the cold rolled state.

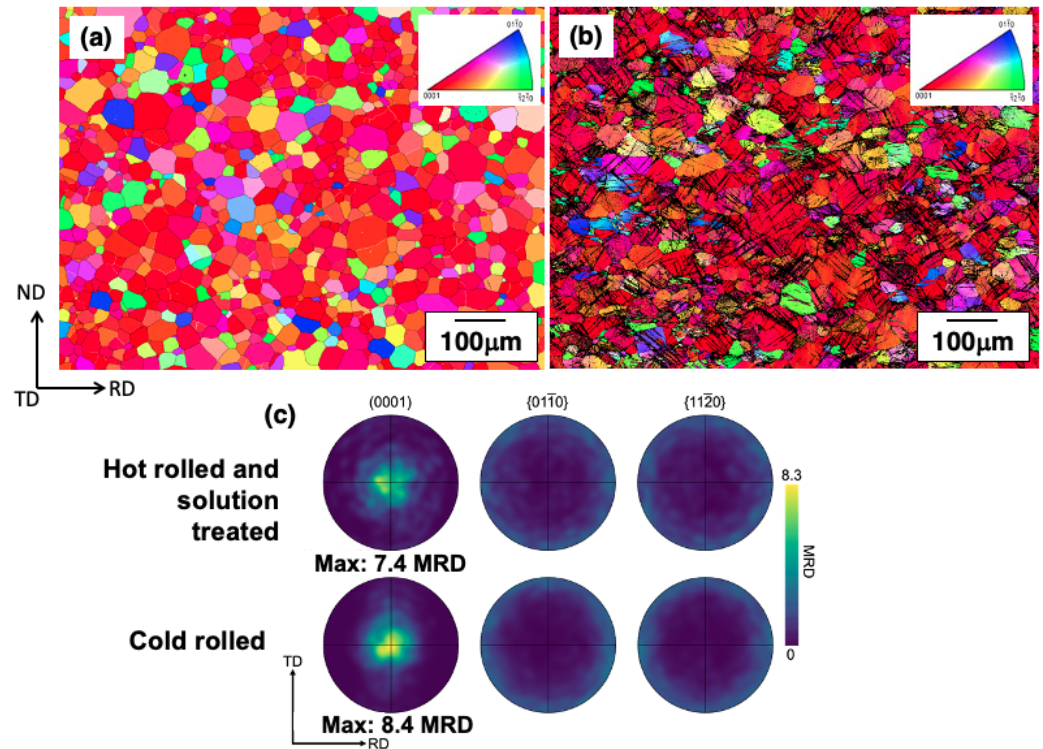


Figure 2. EBSD maps (IPF colouring, normal direction) showing (a) hot rolled and solution treated condition (b) cold rolled condition. (c) Pole figures for the hot rolled + solution treated and cold rolled material.

The SEM images for the solution treated and aged state confirm the optical microscopy observation that the microstructure is fully invaded by DP (Figure 3). In the SEM, the continuous precipitates can be seen as isolated aligned particles on a common habit plane; these are plate shaped with further details of the CP morphology presented elsewhere [6]. The DP regions consist of thicker layers, which are often bent or wavy in appearance and may be broken up into smaller globular regions. However, there is considerable complexity in the detail, with regions of both fine and coarse layer spacing, and significant deviation from the idealized DP structure of continuous parallel layers of uniform thickness on a single habit plane. A higher magnification image (b) shows regions where the DP structures and layer spacings are highly heterogeneous.

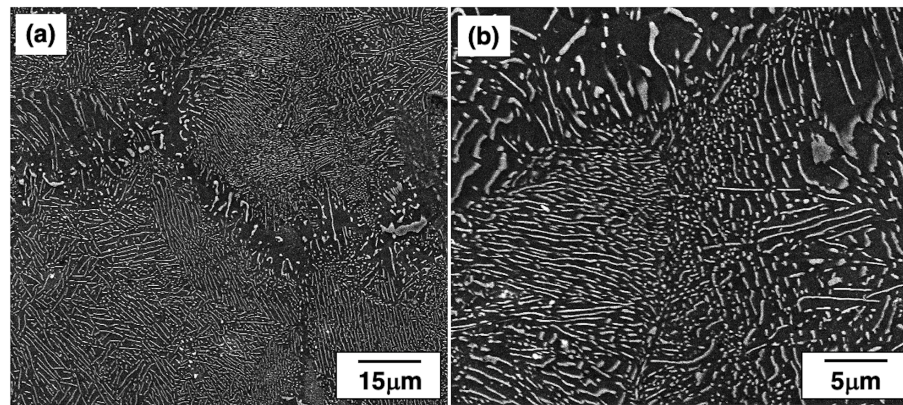


Figure 3. Backscattered SEM images showing the hot rolled, solution treated and aged condition at increasing magnification (a,b).

After cold rolling, the reduced DP fraction observed in the optical micrographs is confirmed by SEM (Figure 4a). Here, most grains contain discrete aligned plate shaped precipitates, typical of the expected CP behaviour in this alloy. However, as observed in the optical images, even after deformation there remain regions of DP in the microstructure. The difference is that these DP regions do not completely invade the grains in which they form. One reason for this is likely to be the promotion of CP by deformation induced defects, as discussed in detail later. However, another obstacle to DP growth are the twin boundaries. An example showing two DP regions that have been blocked from growing in at least one direction by a twin boundary is shown in Figure 4b). The straight red dashed lines superimposed on this micrograph show twin boundaries where there is a sharp transition from a DP to a CP containing region. The twin boundaries are themselves decorated with precipitates aligned along the boundary (with some examples indicated by arrows), but these were never observed to be initiation sites for DP (unlike the precipitates on the normal high angle grain boundaries).

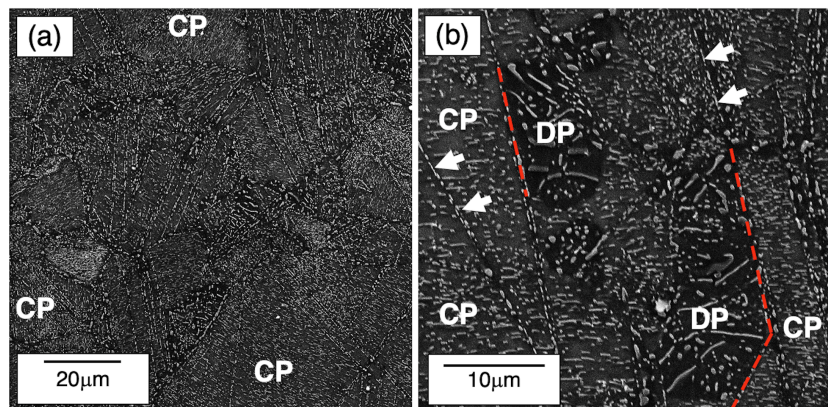


Figure 4. Backscattered SEM images showing the hot rolled, solution treated, cold rolled and aged condition at (a) low magnification and (b) higher magnification, indicating blocking of DP by twin boundaries (red dashed lines) and examples of precipitates on twin boundaries (arrows).

4.2. Precipitation Model

The model was applied to explore the effect of increasing deformation (dislocation density) on the expected precipitation behaviour at 220 °C. The model considers the effect of deformation on the competition between CP and DP but not the direct effect of twin blocking on DP. The significance of this assumption will be discussed later.

Figure 5 shows the predicted evolution of (a) CP and (b) DP volume fraction for aging at 220 °C for different dislocation densities. A dislocation density of 10^{12}m^{-2} corresponds to that expected in a very lightly deformed case, with mean field dislocation densities in

the range $1\text{--}5 \times 10^{14} \text{ m}^{-2}$ reported for heavily deformed AZ alloy at warm temperature (e.g., $150 \text{ }^\circ\text{C}$) [9,10] and higher dislocation densities expected for cold deformation or local regions of strain concentration [11].

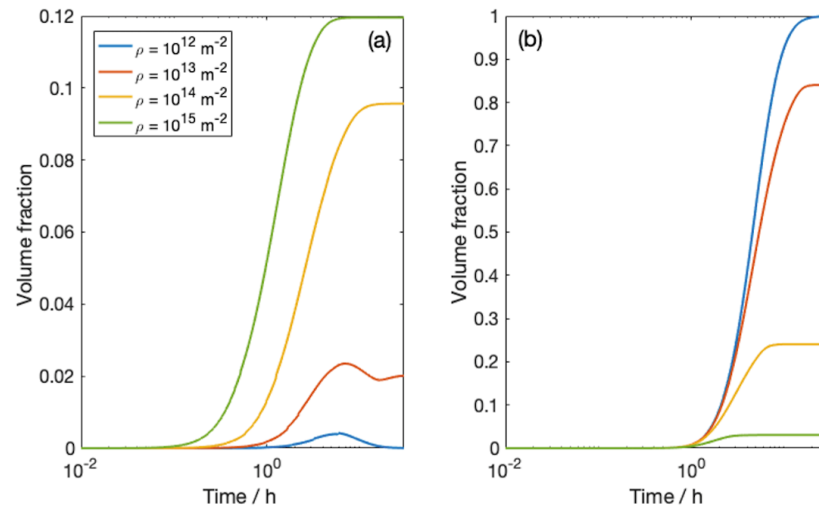


Figure 5. Predictions of the evolution of (a) CP and (b) DP volume fraction for aging at $220 \text{ }^\circ\text{C}$ as a function of dislocation density.

The model demonstrates that at low dislocation densities in the studied range, DP is predicted to dominate, as observed experimentally for undeformed material. As shown in Figure 5a, even at these low dislocation densities, some CP is predicted, but this does not precipitate fast enough to reduce the supersaturation sufficiently to stop DP. Eventually, therefore, this very low volume fraction of CP is predicted to be engulfed by the growing DP. As the dislocation density increases, the faster nucleation of CP leads to an earlier increase in the volume fraction of CP, which both slows the kinetics and reduces the final volume fraction of DP. At a dislocation density of 10^{15} m^{-2} it is predicted that DP is almost completely suppressed and replaced by CP.

This transition from a CP to DP dominated microstructure can be seen more clearly in Figure 6, which shows the volume fractions of the two precipitate types predicted after 16 h at $220 \text{ }^\circ\text{C}$ as a function of dislocation density. The transition between precipitate types is predicted for dislocation densities between around 10^{13} to 10^{15} m^{-2} , which is in the range expected for heavily deformed or cold deformed magnesium alloys [9–11].

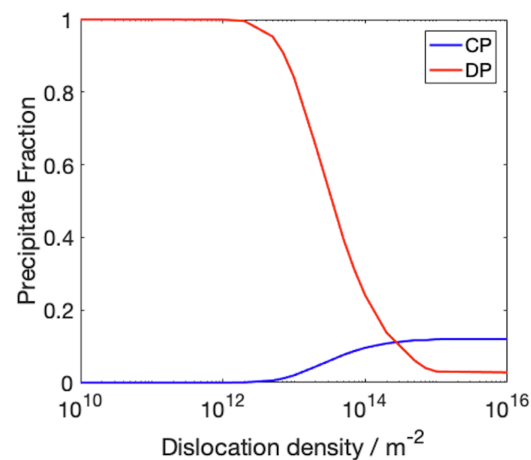


Figure 6. Predicted transition from DP to CP with increasing dislocation density for aging at $220 \text{ }^\circ\text{C}$, 16 h.

To test the ability of the model to estimate the correct influence of dislocations on particle number density and size for CP, it was run for aging at $150 \text{ }^\circ\text{C}$, since this is a case

where measurements have been reported in both deformed and undeformed conditions in the literature [9]. The model predictions of mean radius and number density evolution for CP for aging at 150 °C with and without deformation are compared against the experimental measurements at the end of aging from [9] (Figure 7). As noted in [9], there is likely to be considerable error in both the determination of the experimental dislocation density and particle parameters. Nevertheless, whilst there is some deviation between the predictions and the measurements, it can be seen that the model has captured the correct effect of deformation on the CP kinetics; namely, that the precipitation is greatly accelerated, the particle number density is increased by around an order of magnitude, and the mean particle size is decreased. The model under-predicts the mean particle size in the deformed material, part of this discrepancy is likely to be due to ignoring the effect of dislocations on growth.

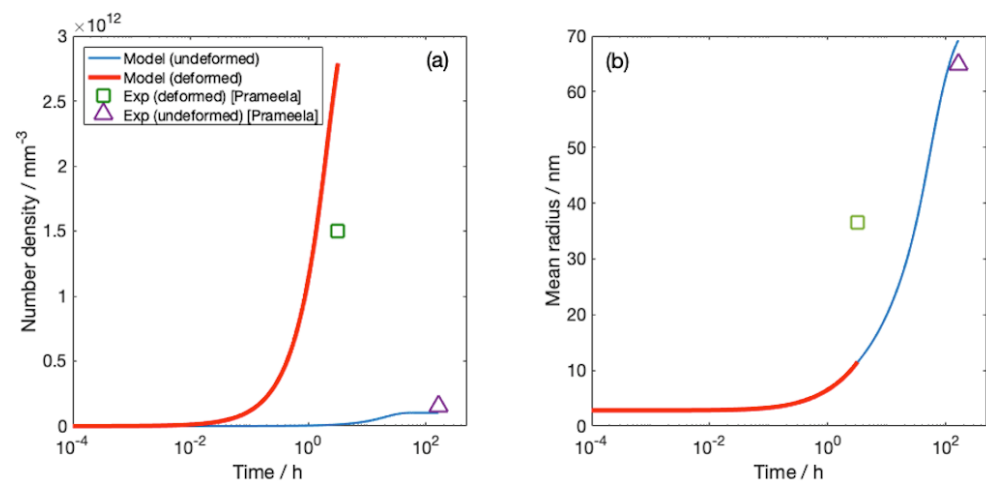


Figure 7. Model predictions of CP number density (a) and mean radius (b) compared with experimental data from [10].

4.3. Deformation Model

The predictions presented so far are based on a mean-field assumption for the dislocation density and solute distribution. This has been shown to give a reasonable prediction of the overall transition from DP to CP dominated behaviour due to deformation consistent with observations. However, additional complexity is introduced by the highly heterogeneous nature of deformation in magnesium alloys and crystal plasticity simulation can help to explore this.

The predicted von-Mises equivalent strain at each voxel point from the DAMASK simulation is shown in Figure 8. As previous simulation and digital image correlation work has demonstrated, the distribution of strains in deformed magnesium alloys is highly heterogeneous. The strain distribution shows “hot spots” that occur in regions adjacent to grain boundaries, where the incompatibility between the deformation of neighbouring grains has to be accommodated. Recalling the applied strain was 5% (plane strain compression), these hot-spots have local strain values of more than twice this, with the maximum recorded as 21%, over 4 times the applied strain.

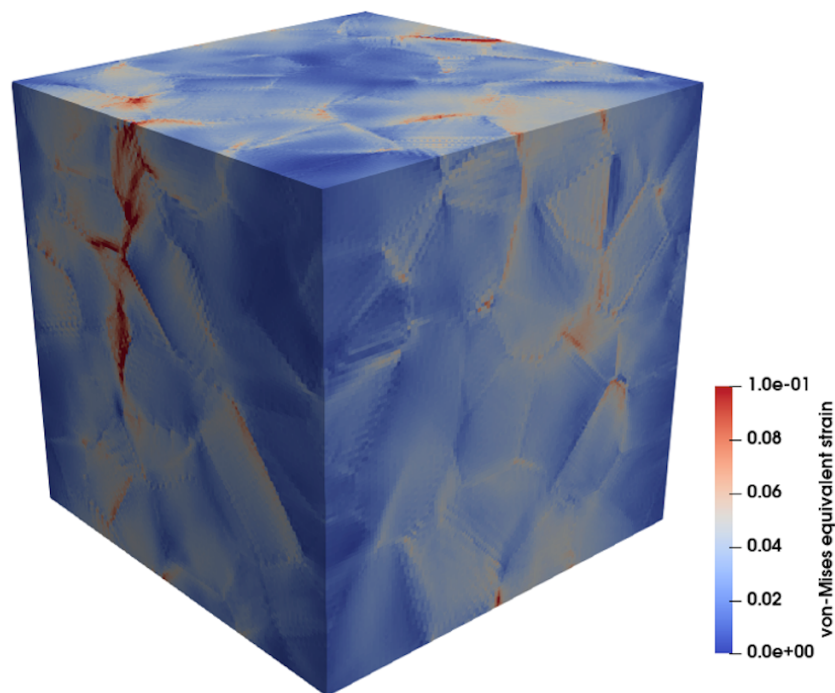


Figure 8. Predicted von-Mises equivalent strain distribution after cold rolling compression using crystal plasticity modelling (DAMASK).

Figure 9a shows a slice through the simulation corresponding to a region containing a band of high local strain (the left-hand face in Figure 8). The local von-Mises equivalent strain along the indicated line through this slice is shown in Figure 9b. The positions of the grain boundaries are marked on the line profile. It can be seen that the regions surrounding the grain boundaries generally have higher local strain and high strain gradients compared to the grain interiors. Furthermore, the strain distribution is usually asymmetric across the boundary. This depends on both the geometric configuration of the boundary and the crystallographic orientation of the neighbouring grains. For the purpose of the present work, the confirmation that strong and asymmetric local strains and strain gradients are expected near to some grain boundaries is important. This will provide a higher local driving force for migration of the grain boundary behind which DP occurs compared to that expected from a mean-field assumption. The significance of this to the observation of patches of DP even after severe deformation [9] will be discussed later.

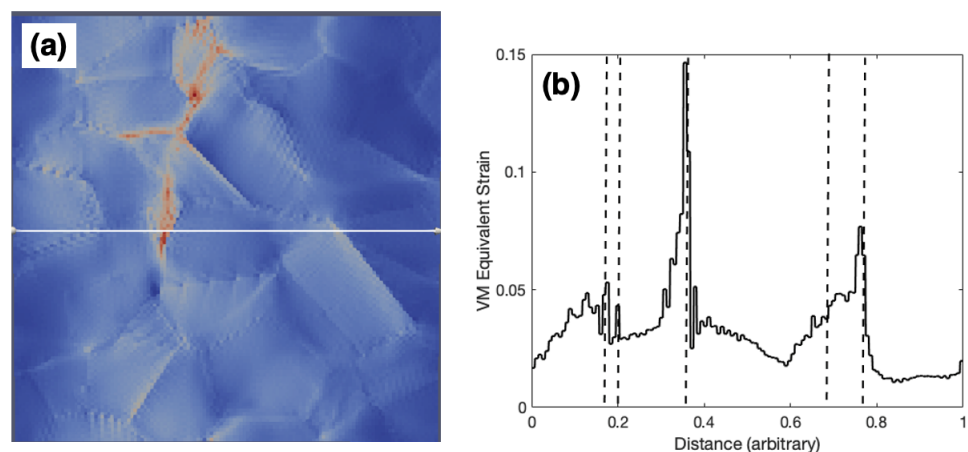


Figure 9. Two dimensional slice through the representative volume element (a) showing line along which local von-Mises equivalent strains are plotted in (b).

5. Discussion

The experimental observations in this work support those of previous studies [8–10], namely that deformation strongly suppresses DP. In regions where DP does not occur, CP is observed. However, it is noteworthy that even after deformation, DP is not completely prevented, but is instead arrested before invading entire grains.

It is also known that deformation does not universally suppress DP in all alloy systems [8]. In some cases, the opposite can occur, and DP can be enhanced by deformation. The precipitation model suggests that strong DP suppression is expected to arise in deformed AZ alloys due to the effect the dislocations have in facilitating nucleation of the continuously formed β precipitates. One of the reasons for the poor age hardening response of AZ alloys despite the potential to reach relatively high precipitate fractions is the difficulty in nucleating these precipitates homogeneously. Dislocations have been shown to be effective nucleation sites for the β phase, enabling much faster nucleation [9,10]. The acceleration of CP reduces the supersaturation available to drive DP, and in AZ magnesium alloys the model predicts this effect easily overcomes that additional driving force for DP due to the stored energy in the deformation substructure.

The enhancement of DP due to deformation (over the driving force due to the supersaturation) can be expressed as an *enhancement factor*, defined as the ratio of the boundary pressure due to the dislocation induced stored energy (P_d) to the stored energy due to the supersaturation (P_c) (Equation (1)). When this factor is small, the contribution of deformation to the DP boundary velocity will be small and vice versa. Figure 10 shows the calculated enhancement factor due to deformation as a function of temperature for three dislocation density values. This is the initial value, before any CP has occurred to reduce P_c or recovery to reduce P_d . As expected, the enhancement factor will be greater when the dislocation density is greater (more stored energy in the deformation structure). However, it can also be seen that the enhancement factor at typical temperatures used for precipitation studies in AZ alloys (150–250 °C) is small (<0.02), even for a very high dislocation density $\rho = 10^{15} \text{ m}^{-2}$. This demonstrates that whilst deformation will enhance the growth velocity of DP, for most practical conditions the effect is small, and is overcome by the faster CP. As temperature increases, the supersaturation decreases, so that P_c becomes smaller and the enhancement factor becomes greater, being asymptotic to the solvus temperature ($P_c = 0$). However, at these high temperatures, recovery will also be very rapid so that any enhancement may not persist for long enough to influence DP growth.

A noteworthy observation in this study, which is consistent with previous work [9], is that even after deformation, DP is not completely suppressed. To understand this, it is necessary to consider the very high level of strain heterogeneity that is typically observed in deformed magnesium, especially at lower temperature (e.g., <200 °C) where non-basal slip system activation is difficult. The crystal plasticity simulations (Figure 8) demonstrate that in the present case, strains in the regions next to the grain boundaries may exceed $4 \times$ the macroscopically applied strain. This leads to an enhanced driving force for DP in the region next to the original grain boundaries, which is exactly coincident with the region where DP starts. Therefore, locally, there can be a much higher driving force for boundary motion, leading to DP in the vicinity of the original grain boundaries before CP becomes established.

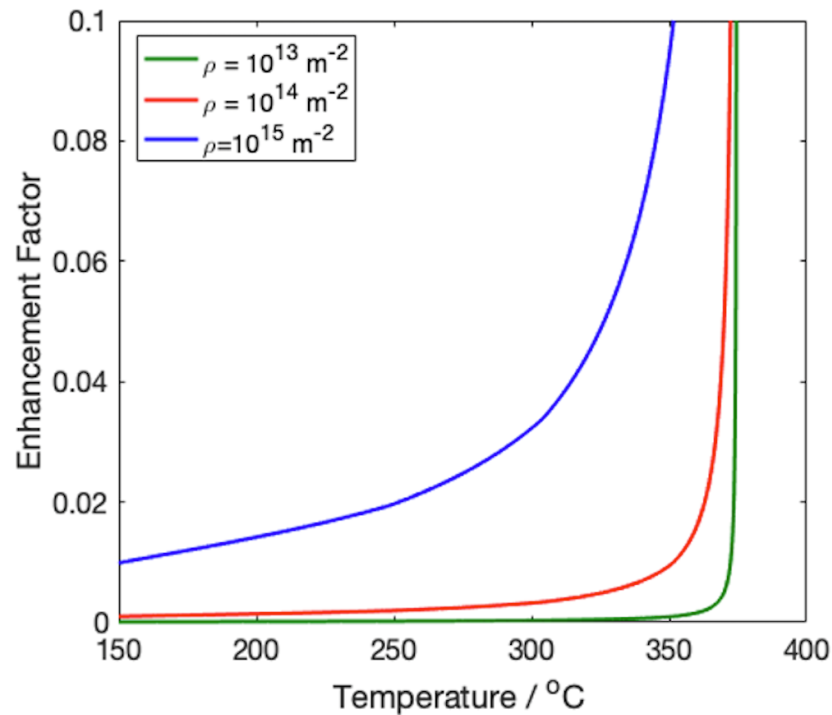


Figure 10. Enhancement to the driving force for DP due to the energy stored in the dislocation sub-structure as a function of aging temperature.

The effect of this on the pressure acting on the DP boundary can be estimated in an approximate way by considering a grain boundary region which contains a linear decrease from a high dislocation density next to the boundary ($3 \times 10^{15} \text{ m}^{-2}$) to a lower dislocation density towards the grain interior ($\rho = 1 \times 10^{14} \text{ m}^{-2}$ at $> 10 \mu\text{m}$ from the boundary). A calculation of the pressure on the DP boundary for this situation at two temperatures is shown in Figure 11. This calculation includes the contribution from the retarding pressure (P_r) due to the additional boundary area created when a hemispherical DP nodule grows out from the original grain boundary (curvature effect). The retarding pressure due to boundary curvature is given by [15]:

$$P_r = \frac{2\gamma_b}{R_d} \quad (3)$$

where γ_b is the high angle grain boundary energy ($\gamma_b = 0.5 \text{ Jm}^{-2}$ [9]) and R_d is the radius of the DP nodule.

It can be seen that only a very small amount of growth is needed to overcome the retarding pressure due to boundary curvature P_r , and the enhancement to DP driving pressure (and therefore growth) will be greatest for boundaries displaced by $\simeq 0.5 \mu\text{m}$. Therefore, small deviations in the boundary (driven by the usual DP nucleation process) will cause displacement of the boundary into a region where its growth becomes enhanced, leading to a local region of DP that is then stopped once the supersaturation ahead of the boundary is reduced significantly by CP. Therefore, although the deformation in the grain boundary regions should also enhance CP nucleation in these regions, this is overcome by the rapid DP that occurs by small displacements of the grain boundary before CP becomes established. Solute depletion in the grain boundary regions due to grain boundary precipitation may also play a role by reducing the supersaturation available for CP nucleation.

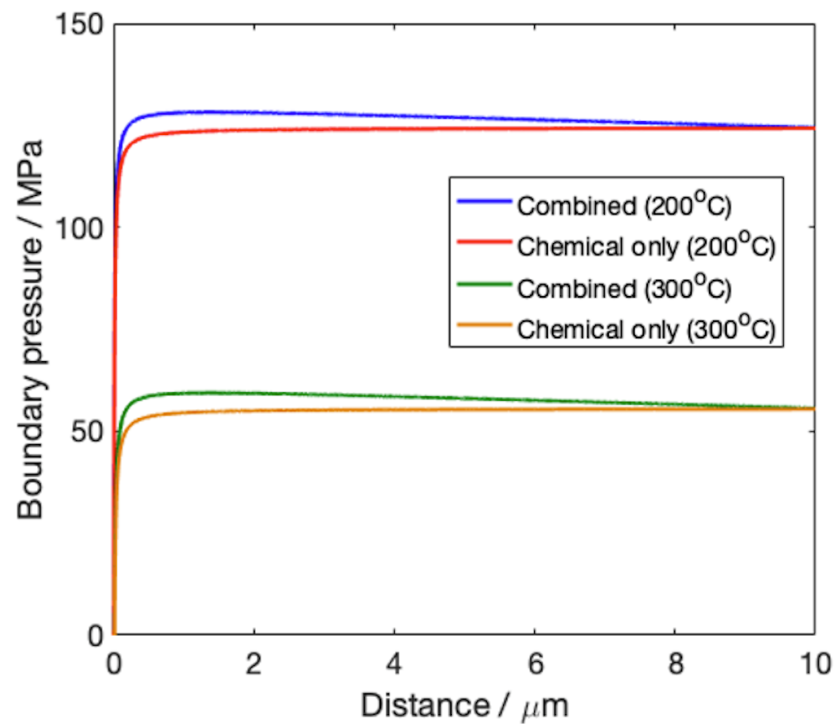


Figure 11. Pressure driving the migration of the DP growth front considering a reduction in the local stored energy due to the dislocation sub-structure as a function of distance from the original boundary position.

Finally, the direct role of twins in blocking DP can be considered. As demonstrated in the present study, twin boundaries and twin tips can provide impenetrable boundaries to DP growth. Twins formed within a grain therefore restrict the region into which DP can grow from a single nucleation event, as demonstrated schematically in Figure 12a,b. However, multiple nucleation events can still lead to complete invasion of the grain (apart from in twin interiors, where DP was not observed) as shown schematically in Figure 12c,d. In the case that the twins are very narrow compared with the grain size (as in the cold rolled material used in this study) the lack of DP within the twinned material itself has only a small effect on the DP volume fraction and can be ignored in a simple analysis. Instead, the direct effect of twin blocking on the DP fraction can be simply estimated by modifying the effective number of nuclei per grain. This is because a twin will effectively divide a single grain into two grains (ignoring the twin interior), but without introducing any new nucleation sites for DP, since twin boundaries cannot nucleate DP. In a twin free grain, one nucleus formed per grain is sufficient to produce complete invasion of the grain by DP (ignoring the competition from CP). When one twin is present, at least two nuclei per grain are required, and so on for increasing numbers of twins in each grain.

Although the details of this effect are complicated, especially in the case of intersecting twins on different planes and twins that terminate inside the grain, a very simple modification to the model was made to consider the approximate direct suppression effect due to twins by decreasing the effective nucleation rate per grain with an increasing number of twins. Turning off CP in the model, so the effect of depletion of supersaturation is ignored, the direct effect of twins on the DP volume fraction evolution predicted at 220 °C is shown in Figure 13. As expected, twins will slow the overall kinetics, but the effect is quite small compared to the very strong effect of CP in depleting the available solute (discussed previously). However, it is likely that the slowing of kinetics of DP also contributes to the additional CP that forms in the deformed case, since the two mechanisms are in competition for the untransformed volume.

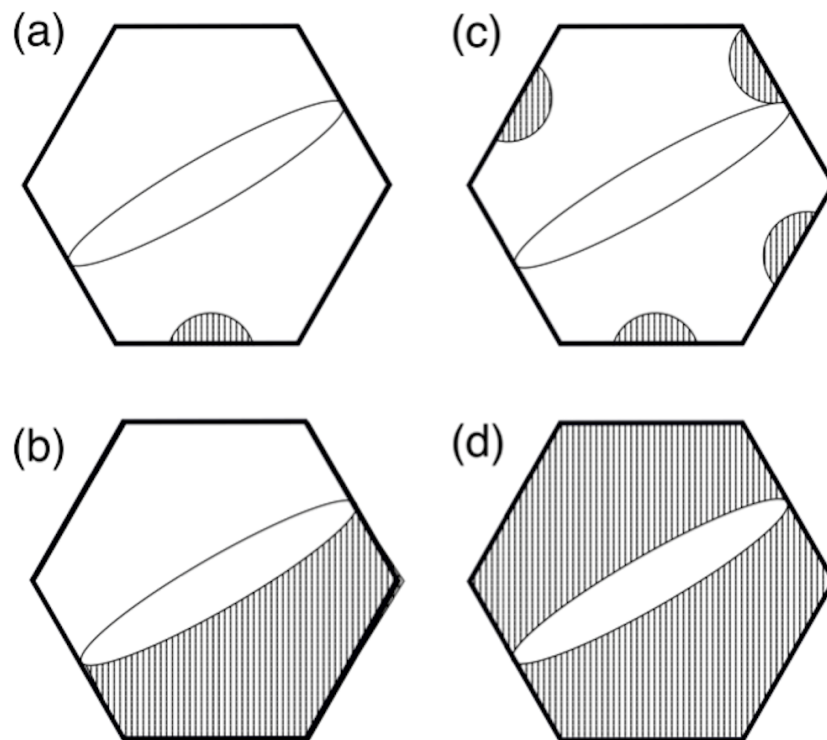


Figure 12. Schematic showing how DP can evolve in a grain containing a twin assuming no competition from CP. DP regions are indicated with a shaded pattern. (a,b) Single nucleation site active, (c,d) multiple nucleation sites active.

Overall, the model suggests that the dominant effect of deformation is in the promotion of CP, reducing the supersaturation for DP so that it stalls early in the precipitation process. Other evidence supporting this point is that DP is suppressed after deformation even in grains which do not contain twins, as observed in the micrographs in this study and also in previous work [8].

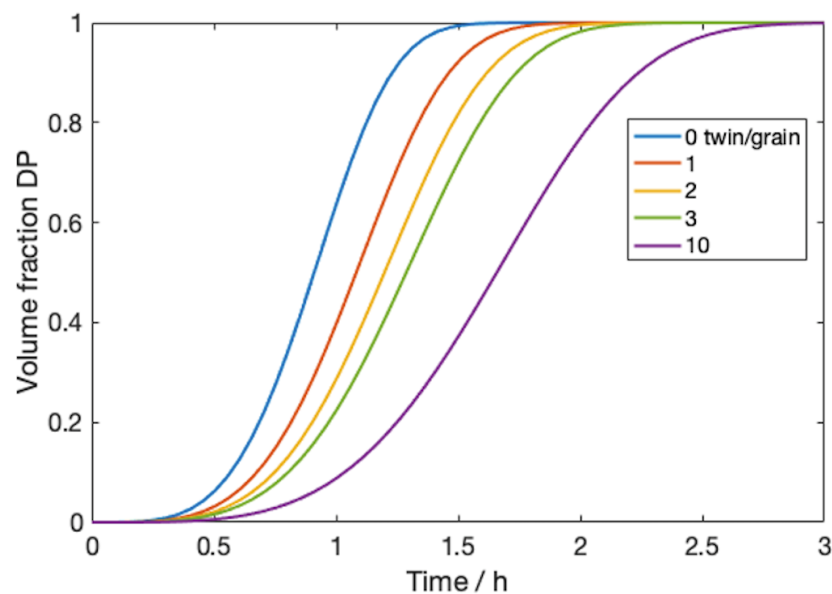


Figure 13. Prediction of the effect of twin blocking on the kinetics of DP volume fraction evolution assuming no competition from CP.

6. Conclusions

The effect of deformation on the competition between continuous (CP) and discontinuous (DP) precipitation modes in AZ magnesium alloys has been investigated. An existing mean-field model has been extended to predict the effect of deformation on this competition and to help understand why deformation is seen to strongly suppress DP in these alloys. Crystal plasticity modelling has also been used to explore the important effect of microstructural heterogeneity, which is not captured in the mean-field model. The following conclusions may be drawn from this work:

1. Consistent with previous studies, cold rolling was found to strongly suppress DP and promote CP after aging under conditions that lead to a fully DP microstructure in the solution treated and aged condition.
2. The model predicts that the dominant effect of deformation is to promote the nucleation of CP on dislocations, which rapidly reduces the supersaturation and therefore the driving force for DP, causing it to stall.
3. Even after deformation, some regions of DP persist close to the original grain boundaries. Crystal plasticity modelling demonstrates that this corresponds to regions where high levels of strain localization are expected, which provides an enhanced driving force for DP at the exact location where the initial DP nodules nucleate. This may allow limited DP to occur in these regions before CP can become established.
4. Twins also directly suppress DP by acting as hard obstacles that block the growth of DP nodules. However, the effect of twinning alone on suppressing DP is predicted to be less than the effect of the reduced supersaturation due to promotion of CP by deformation. By delaying the DP transformation, twins may also enable more CP nucleation and growth, which itself will further retard DP.

Author Contributions: Conceptualization, J.R.; methodology, J.R., J.G. and A.D.; software, J.R.; formal analysis, J.R., J.G. and A.D.; investigation, J.R., J.G. and A.D.; writing—original draft preparation, J.R.; writing—review and editing, J.R., J.G. and A.D.; visualization, J.R.; supervision, J.R.; project administration, J.R.; funding acquisition, J.R. All authors have read and agreed to the published version of the manuscript.

Funding: This research was funded by EPSRC LightForm grant number EP/R001715/1. J.R. thanks the Royal Academy of Engineering/DSTL for funding through the RAEng/DSTL Chair in Alloys for Extreme Environments.

Institutional Review Board Statement: Not applicable.

Informed Consent Statement: Not applicable.

Data Availability Statement: The data required to reproduce these findings are available from the EPSRC LightForm Zenodo repository (<https://zenodo.org/communities/lightform>, accessed on 11 March 2022).

Acknowledgments: Luxfer MEL are thanked for the provision of the materials used in this study. Pratheek Shanthraj is thanked for help with the use of the DAMASK crystal plasticity software.

Conflicts of Interest: The authors declare no conflict of interest.

References

1. Christian, J.W. *The Theory of Transformations in Metals and Alloys*; Elsevier: Amsterdam, The Netherlands, 2002.
2. Williams, D.; Butler, E. Grain boundary discontinuous precipitation reactions. *Int. Met. Rev.* **1981**, *26*, 153–183. [[CrossRef](#)]
3. Zener, C. Kinetics of the decomposition of austenite. *Trans. AIME* **1946**, *167*, 550–595.
4. Hillert, M. On theories of growth during discontinuous precipitation. *Metall. Mater. Trans. B* **1972**, *3*, 2729–2741. [[CrossRef](#)]
5. Klinger, L.M.; Brechet, Y.J.M.; Purdy, G.R. On velocity and spacing selection in discontinuous precipitation—I. simplified analytical approach. *Acta Materialia* **1997**, *45*, 5005–5013. [[CrossRef](#)]
6. Hutchinson, C.R.; Nie, J.-F.; Gorsse, S. Modeling the precipitation processes and strengthening mechanisms in a Mg–Al–(Zn) AZ91 alloy. *Metall. Mater. Trans. A* **2005**, *36*, 2093–2105. [[CrossRef](#)]
7. Robson, J. Modeling competitive continuous and discontinuous precipitation. *Acta Material.* **2013**, *61*, 7781–7790. [[CrossRef](#)]

8. Duly, D.; Audier, M.; Brechet, Y. On the influence of plastic deformation on discontinuous precipitation in Mg–Al. *Scr. Metall. Material.* **1993**, *29*, 1593–1596. [[CrossRef](#)]
9. Ma, X.; Prameela, S.E.; Yi, P.; Fernandez, M.; Krywopusk, N.M.; Kecskes, L.J.; Sano, T.; Falk, M.L.; Weihs, T.P. Dynamic precipitation and recrystallization in Mg-9wt.%Al during equal-channel angular extrusion: A comparative study to conventional aging. *Acta Material.* **2019**, *172*, 185–199. [[CrossRef](#)]
10. Prameela, S.E.; Yi, P.; Medeiros, B.; Liu, V.; Kecskes, L.J.; Falk, M.L.; Weihs, T.P. Deformation assisted nucleation of continuous nanoprecipitates in Mg–Al alloys. *Materialia* **2020**, *9*, 100583. [[CrossRef](#)]
11. Shi, G.; Yuan, J.; Li, T.; Zhang, K.; Li, X.; Li, Y.; Ma, M. Enhanced precipitation strengthening of extruded Mg-8 wt.%Al-0.5wt.%Zn (AZ80) magnesium alloy by extension twinning. *Mater. Sci. Eng. A* **2020**, *774*, 138906. [[CrossRef](#)]
12. Tu, K.-N.; Turnbull, D. Morphology of cellular precipitation of tin from lead-tin bicrystals. *Acta Metall.* **1967**, *15*, 369–376. [[CrossRef](#)]
13. Orozco-Caballero, A.; Lunt, D.; Robson, J.D.; da Fonseca, J.Q. How magnesium accommodates local deformation incompatibility: A high-resolution digital image correlation study. *Acta Material.* **2017**, *133*, 367–379. [[CrossRef](#)]
14. Roters, F.; Diehl, M.; Shanthraj, P.; Eisenlohr, P.; Reuber, C.; Wong, S.; Maiti, T.; Ebrahimi, A.; Hochrainer, T.; Fabritius, H.-O.; et al. DAMASK—The Düsseldorf advanced material simulation kit for modeling multi-physics crystal plasticity, thermal, and damage phenomena from the single crystal up to the component scale. *Comput. Mater. Sci.* **2019**, *158*, 420–478. [[CrossRef](#)]
15. Humphreys, F.J.; Hatherley, M. *Recrystallization and Related Annealing Phenomena*; Elsevier: Amsterdam, The Netherlands, 2004.